



Effect of Substrate Concave Pattern on Splat Formation of Yttria-Stabilized Zirconia in Atmospheric Plasma Spraying

Kentaro Shinoda, Mehdi Raessi, Javad Mostaghimi, Toyonobu Yoshida, and Hideyuki Murakami

(Submitted June 4, 2009; in revised form July 14, 2009)

Splat morphology of yttria-stabilized zirconia (YSZ) on a microconcave-patterned substrate was investigated by both numerical and experimental approaches under a dc-rf hybrid-plasma spray condition. The spreading behavior of molten droplets on a microdimple pattern was numerically simulated in a three-dimensional form. For comparison, impact of a YSZ droplet onto a microdimple pattern of a quartz glass substrate was studied in situ utilizing thermal emissions from the droplet. Concave aspects of a substrate surface play an important role in fingering/splashing of a spreading droplet as well as convex patterns. The main mechanism that causes splashing is likely due to the slipping of a spreading droplet at the edge of concave patterns. The viscosity decrease of the spreading droplet enhances the droplet splash.

Keywords coatings for gas turbine components, coating-substrate interaction, diagnostics and control, influence of process parameters, roughness effects, splats cooling, spray deposition

1. Introduction

Surface roughness of the substrate is one of the most important parameters in determining the microstructure and properties of plasma-sprayed coatings. Although the surface roughness increases the adhesion strength of the coating to the substrate, it may result in the deterioration of the coating due to the splashing of impinging droplets. Therefore, it is important to fully understand the effect of the surface roughness on the single splat and subsequent coating formations (Ref 1, 2).

In our previous paper (Ref 3), we studied alumina splat morphology on various micropatterned substrates under hybrid plasma spray conditions. We showed that the splat morphology was affected by surface patterns in which the ratio of the arithmetic surface roughness R_a to the droplet diameter was as small as 0.02. We also found that the

fingering of alumina splats occurred on both concave- and convex-patterned substrates, where we define the convex and concave patterns as follows: the convex pattern is a plane that has more than one convex object on its surface; the concave pattern is a plane that has more than one concave object on its surface. McDonald et al. (Ref 4) photographed and measured cooling rates of molten nickel and molybdenum droplets impinging on silicon wafers textured with columnar objects. They found that the cooling rate of spreading droplets was related to the width of inter-columnar spacing. When the spreading droplet filled inter-columnar spaces, columns acted as fins, promoting splat cooling (Ref 5). Parizi et al. (Ref 6) conducted numerical simulations for molten nickel and yttria-stabilized zirconia (YSZ) droplets impinging on textured silicon wafers and compared their results with the experiments of McDonald et al. (Ref 4). They confirmed that the change in splat shapes on patterned surfaces was due to the rapid solidification, as predicted by Raessi et al. (Ref 7). Thus, the effect of convex patterns on splat formation and morphology has been studied relatively well. However, the effect of concave patterns has not received much attention and is not well understood.

Understanding the roughness effects including concave patterns requires the complementary approach by both numerical simulations and experiment. Although some excellent numerical simulations had been reported on this issue (Ref 8, 9), the lack of in situ experimental data made it difficult to closely link the numerical studies with the experimental studies. In this regard, the primary work by Parizi et al. mentioned above (Ref 6) is a milestone study to fill in the gaps between the numerical simulations and the experimental works. In other word, the recent development in experimental studies enabled us the collaborative research between numerical simulation and experiment.

Kentaro Shinoda and **Hideyuki Murakami**, Hybrid Materials Center, National Institute for Materials Science (NIMS), 1-2-1 Sengen, Tsukuba, Ibaraki 305-0047, Japan; **Mehdi Raessi** and **Javad Mostaghimi**, Centre for Advanced Coatings Technologies, Department of Mechanical and Industrial Engineering, University of Toronto, Toronto, ON M5S 1A4, Canada; and **Toyonobu Yoshida**, Department of Materials Engineering, Graduate School of Engineering, University of Tokyo, 7-3-1 Hongo, Bunkyo-ku, Tokyo 113-8656, Japan. Contact e-mail: shinoda.kentaro@nims.go.jp.

In this paper, we investigate the spreading phenomena of YSZ droplets on concave-patterned substrates deposited by the dc-rf hybrid plasma spraying. We simulated the spreading behavior of molten YSZ droplets on dimple-patterned substrates representing concave patterns using a three-dimensional numerical model. We also conducted an in situ measurement of the spreading behavior of YSZ droplets on a dimple-patterned substrate made by a wet-etching technique.

2. Numerical Analysis

2.1 Numerical Methods

Three-dimensional numerical simulations were conducted to investigate the splat formation of YSZ droplets on a dimple-patterned substrate made of quartz glass. The details of the numerical model were given elsewhere (Ref 10, 11), and are briefly described here. Assuming incompressible and Newtonian fluid, the conservation of mass, momentum, and energy equations were solved for the droplet by considering phase change (solidification) (Ref 11). The effect of surrounding gas was neglected. In addition, the heat transfer inside the substrate and the solidified layer was also modeled. To solve the energy equation, the enthalpy transforming model (Ref 12) was used to convert the energy equation to a single-variable (enthalpy) equation. The term of undercooling (Ref 13) was not included in this study.

The dimple-pattern geometry used for simulations is shown in Fig. 1. Each dimple was 8 μm in diameter and 1 μm in depth. The dimples were arranged as triangular lattice position; the distance between lattice points was 10 μm . The dimples covered approximately 58% of the substrate area.

Table 1 summarizes physico-chemical properties used in the calculation (Ref 14-17). The contact angle of the YSZ droplet on a quartz glass substrate was assumed to be 90° due to the lack of the data; this is not expected to influence the results, as it was reported that the contact angle does not affect the splat spreading when the impact velocity is larger than 1 m/s (Ref 18). Thermal contact

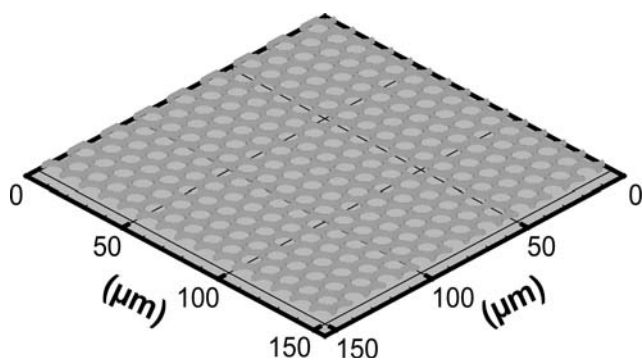


Fig. 1 Dimple-pattern geometry used for simulations. Circle regions are concaves

resistance of the region where the spreading droplet was in contact with the substrate was assumed to be zero. This may increase the solidification effect on spreading at these regions, but the effect is not significant in the case of YSZ (Ref 19). Note that this assumption does not mean that the overall thermal contact resistance is always zero. If a droplet is spreading without filling dimples, the contact area decreases, resulting in higher thermal contact resistance.

Table 2 summarizes the initial conditions used in the calculations. The diameter, velocity, temperature, and the Reynolds number Re of the droplet were 57 μm , 43 m/s, 2951 K, and 471, respectively, which were comparable to experimental data presented later. The substrate temperature was set to 700 K.

2.2 Numerical Results

Figure 2(a) and (b), respectively, show the computer-generated images of final shapes (50 μs after the impact) of the splat on the smooth substrate (SOS) and the splat on the dimple-patterned substrate (SOD). The images of the SOD (6 μs after the impact) whose droplet impacted at the same impact conditions, but the kinematic viscosity was halved, i.e., $\nu = 2.6 \times 10^{-6} \text{ m}^2/\text{s}$ and $Re = 943$, is also shown in Fig. 2(c). The former two splats ($Re = 471$) were disk-shaped, even though the rim of the SOD exhibited perturbations. Meanwhile, the latter SOD ($Re = 943$) exhibited splashing. In both cases on the dimple-patterned substrate, splat did not fill dimples completely. The diameters of the SOS and SOD ($Re = 471$) were 162 and

Table 1 Physico-chemical properties used in this study

Properties	Values	References
Melting point, T_m , K	2950	Ref 14
Fluid density, ρ_f , kg/m^3	4300	Ref 15
Specific heat of fluid, c_f , J/kg K	713	Ref 14
Thermal conductivity of fluid, k_f , W/mK	2.32	Ref 16
Kinematic viscosity of fluid, ν , m^2/s	5.2×10^{-6}	Ref 17
Surface tension of fluid, σ , N/m	0.43	Ref 15
Latent heat of fusion, H_f , kJ/kg	706	Ref 14
Specific heat of solid, c_s , J/kg K	604	Ref 14
Thermal conductivity of solid, k_s , W/m K	2.32	Ref 16
Density of substrate, ρ_{sub} , kg/m^3	2000	Ref 16
Specific heat of substrate, c_{sub} , J/kg K	900	Ref 16
Thermal conductivity of substrate, k_{sub} , W/m K	1.8 at 700 K	Ref 16

Table 2 Initial conditions for numerical simulation

Parameters	Values
Diameter, d_o , μm	57
Velocity, V_o , m/s	43
Temperature, T_o , K	2951
Substrate temperature, T_{sub} , K	700
Contact angle, θ , °	90
Thermal contact resistance, R_{TC} , $\text{m}^2 \text{ K}/\text{W}$	0
Reynolds number, Re	471
Weber number, We	1054

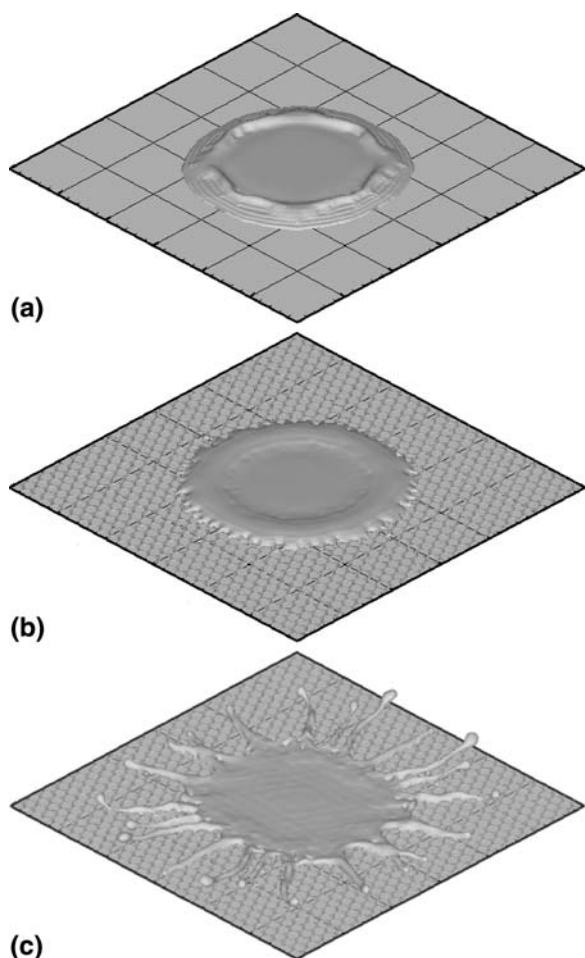
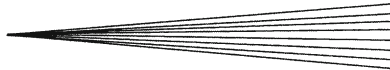


Fig. 2 Computer-generated images of YSZ splats (a) on a smooth substrate (the Reynolds number, $Re=471$; $50 \mu\text{s}$ after impact), (b) on a dimple-patterned substrate ($Re=471$; $50 \mu\text{s}$ after impact), (c) on a dimple-patterned substrate ($Re=943$; $4 \mu\text{s}$ after impact). One division corresponds to $50 \mu\text{m}$

$171 \mu\text{m}$, respectively; hence, the degrees of flattening, ξ , were 2.8 and 3.0, respectively. The average diameter of the perturbed splat was used here as the diameter of the SOD.

Figure 3 shows the evolutions of the droplet shapes at the spreading stage. As we can see, when $Re=943$, the droplet splashed on the dimple-patterned substrate; however, on the smooth substrate, we still obtained a disk-shaped splat, although the rim of the splat was slightly perturbed. It is interesting that the SOD show perturbations on the rim either when $Re=471$ or 943 , at the initial stages of impact ($t=0.5 \mu\text{s}$) as shown at the bottom of Fig. 3. However, the perturbations at $Re=471$ did not result in splashing.

The diameter evolution of droplets shown in Fig. 3, and the corresponding spread velocity are plotted in Fig. 4. The spread velocity was calculated at the advancing front of the spreading droplets from the rate of spreading obtained from numerical simulations. The velocity was then averaged at the time intervals shown in Fig. 3. The fastest and slowest positions were calculated. First, the



spreading behaviors of the SOD and SOS at the same Reynolds number $Re=943$ are compared. At the beginning of the spread ($0 < t < 0.5 \mu\text{s}$), there was no distinct difference seen in the spreading of droplets on the dimple-patterned and smooth substrates. At this stage, the spread velocity nearly reached 200 m/s , which is almost five times higher than the impact speed. At $0.5 < t < 1.0 \mu\text{s}$, some regions on the periphery of the droplet on the dimple-patterned substrate were slowed down rapidly compared to that on the smooth substrate. Finally, during $1.0 < t < 4.0 \mu\text{s}$, advancing fingers of the SOD kept on spreading with small deceleration, while other parts of the SOD stop spreading. At $Re=471$, the spread behavior of the SOD was similar to that of the SOS as the splat shape indicated.

3. Experiment

3.1 Experimental Methods

An in situ measurement system developed previously (Ref 17, 20) was used to study the droplet impact on a dimple-patterned substrate under the dc-rf hybrid plasma spraying (Ref 21, 22). This system can obtain single splats on the substrate utilizing orifices and can correlated splat morphology with the impact condition such as the diameter, velocity, and temperature of the impacting droplet and the thermal radiation history during the impact one-to-one. The thermal radiation of the impacting droplet was measured with photomultiplier tubes filtered by $700/1000 \text{ nm}$ wavelength narrow band pass filters via a condenser lens. Note that the angle between the substrate and the condenser lens was 20° . Droplet overall temperature during impact was derived from $700/1000 \text{ nm}$ wavelengths by two-color pyrometry, and cooling rates were defined as the maximum temperature gradient during impingement.

Conventional fused and crushed 8 wt.% YSZ powder with size ranging from 63 to $88 \mu\text{m}$ (similar to K-90, Showa Denko K.K., Tokyo, Japan) were deposited via the 8 vol.% $\text{H}_2\text{-Ar}$ hybrid plasma spraying. The spray conditions were the same as those in the previous study (Ref 20). Two kinds of quartz glass substrates were used: a smooth ($R_a=0.04 \mu\text{m}$) substrate and a microdimple-patterned substrate ($R_a=-0.5 \mu\text{m}$). Figure 5 shows the laser-scanning microscope image of the dimple-patterned substrate, which was made by wet-etching technique. Details of the manufacturing process are described elsewhere (Ref 3). The arrangement of dimple patterns was the same as the simulation, except that the depth of dimples was $0.5 \mu\text{m}$. The substrate temperature in both cases was kept at approximately 700 K , at which splats are expected to form a disk shape on a smooth substrate (Ref 23).

In previous studies (Ref 17, 23), we measured the volume of a splat and then calculated the initial droplet diameter assuming that the droplet was initially a solid sphere. However, since the volume measurement of SODs might have errors due to dimples, we used it in conjunction with another measurement technique; that is, assuming droplets to be gray body, we calculated the

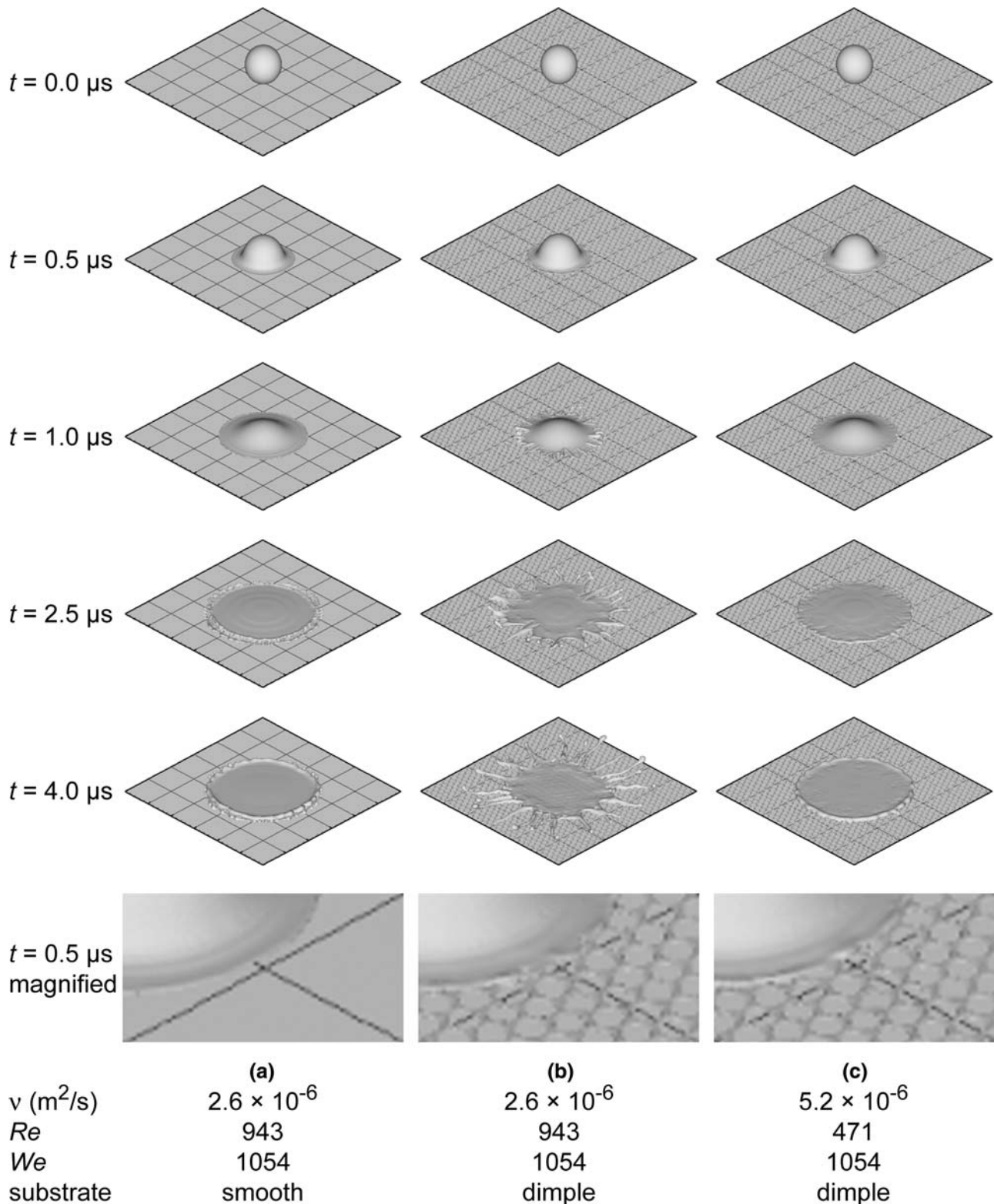
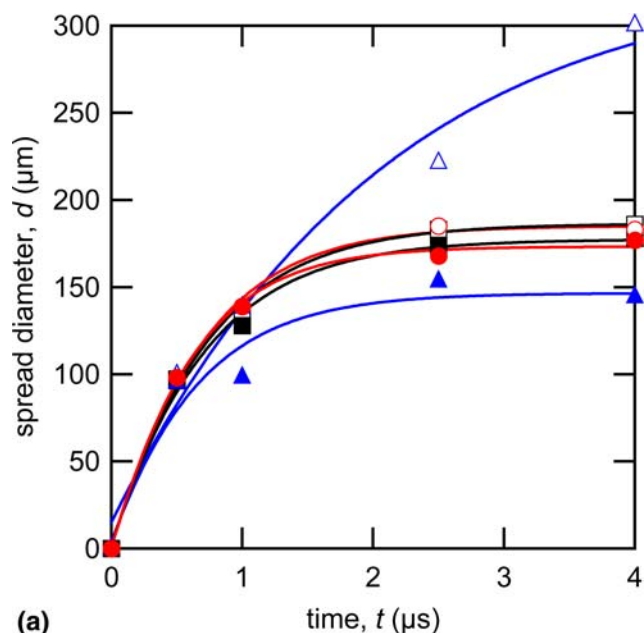
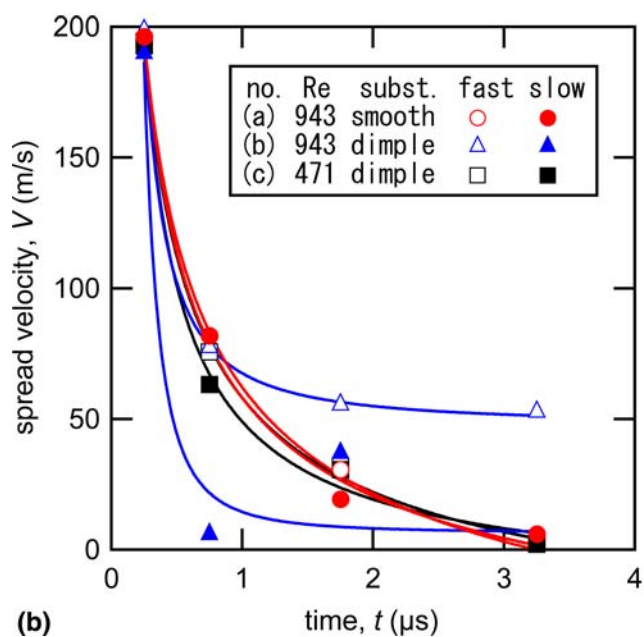


Fig. 3 Time evolution of computer-generated images of YSZ droplets in the case of (a) on a smooth substrate, with the kinematic viscosity, $\nu = 5.2 \times 10^{-6} \text{ m}^2/\text{s}$, the Reynolds number $Re = 943$, the Weber number $We = 1054$, (b) on a dimple-patterned substrate, with $\nu = 2.6 \times 10^{-6} \text{ m}^2/\text{s}$, $Re = 943$, $We = 1054$, and (c) on a dimple-patterned substrate, with $\nu = 5.2 \times 10^{-6} \text{ m}^2/\text{s}$, $Re = 471$, $We = 1054$ at time $0 < t < 4.0 \mu\text{s}$. The magnified views of lower right part of the droplets at $t = 0.5 \mu\text{s}$ are also shown in the bottom



(a)



(b)

Fig. 4 Spread diameter d and spread velocity V of impacting droplets as a function of spread time t for the droplets (a) the Reynolds number $Re = 943$ on a smooth substrate, (b) $Re = 943$ on a dimple substrate, and (c) $Re = 471$ on a dimple substrate, calculated from the computer-generated images in Fig. 3. Fast and slow indicate the calculated positions at which the spreading velocities are fastest and slowest, respectively (color online)

droplet diameters from thermal emission intensity of the droplets. The droplet sizes of in-flight particles shown here were calibrated by comparing with the diameter calculated from the splat volume as shown in Fig. 6. The standard deviation was 17% for 78 disk-shaped splats on a preheated smooth substrate. Although some droplet diameters contained large error, they were consistent with each other. Therefore, the calculated diameter from

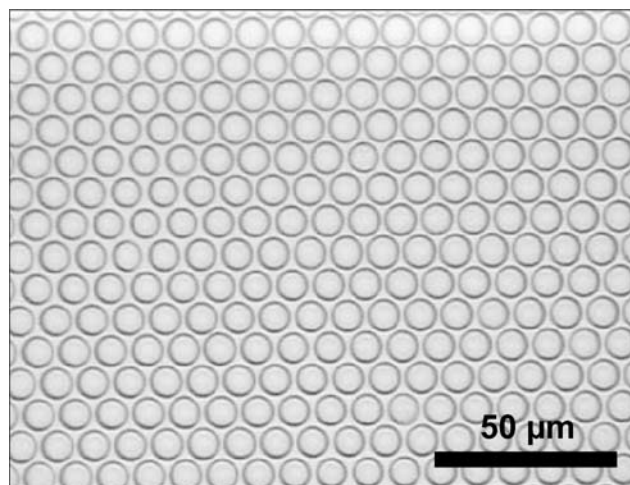


Fig. 5 Laser-scanning microscope view of a microdimple-patterned quartz glass substrate made by wet-etching technique used for the experiment. Circle regions are the concaves of $0.5 \mu\text{m}$ in depth

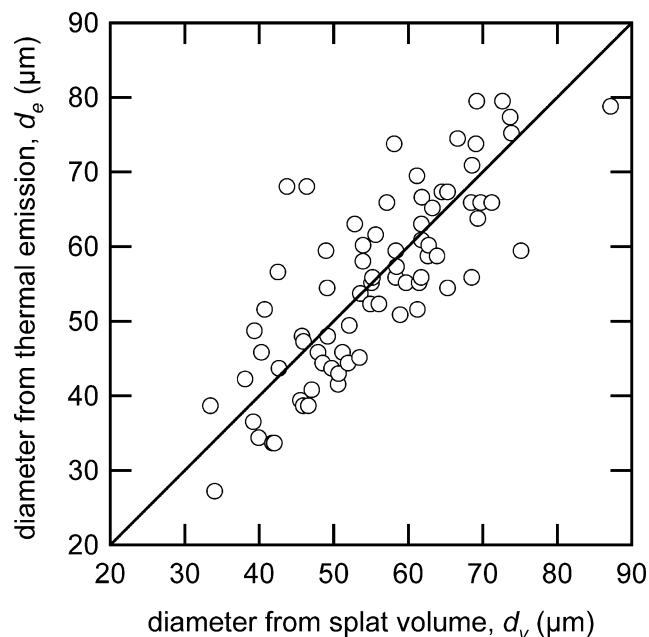


Fig. 6 Comparison of droplet diameters derived from thermal emissions of in-flight droplets, d_e , and those derived from the splat volume, d_v

in-flight emission signals were rather reliable and can be applied to estimate the volume of a splashing SOD, which is difficult to measure by the laser-scanning microscope.

3.2 Experimental Results

All the SODs had a disturbed and distorted rim and showed fingering and/or splashing shapes as shown Fig. 7(a). Compared to alumina splats shown in Fig. 7(b), which was adapted from our previous paper (Ref 3), YSZ

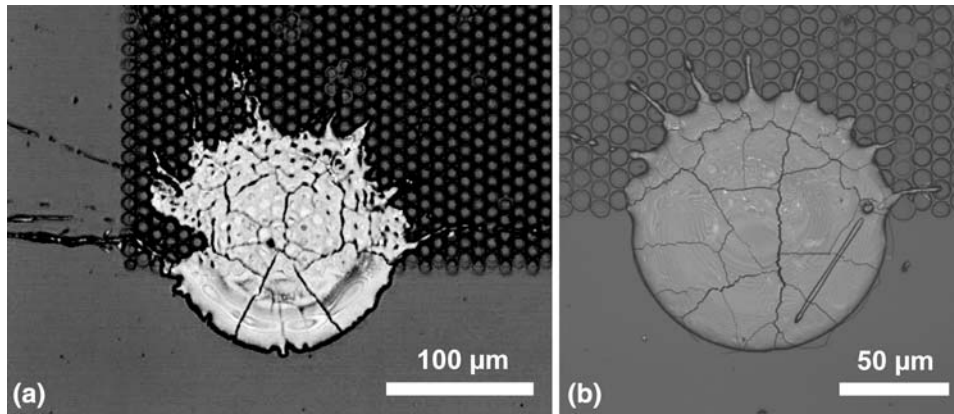


Fig. 7 Laser-scanning microscope images of splats deposited on the boundary between dimple pattern and smooth region: (a) YSZ and (b) alumina. The image of alumina was adopted from Fig. 7 (b2) of the work Shinoda et al. (Ref 3)

splats had a tendency to flatten more and to show fingering and/or splashing more on the same dimple-patterned substrates. The degrees of flattening of the YSZ splats (3-5) were larger than those of alumina splats (2.5-3.5), even though the impact velocities of the YSZ droplets (30-70 m/s) in this study were lower than those of alumina droplets (~90 m/s) (Ref 3). This is probably due to the lower viscosity of YSZ compared to alumina as was reported (Ref 17). The rim of the splat on the region of the dimple pattern was less rounded and flatter than that on the smooth region. Dimples that located under the middle to peripheral region of the splat were not fully filled by the splat, which was similar to the case of alumina splats (Ref 3), suggesting that the droplet spread over the dimple-pattern substrate without filling these dimples at least in the later stage of spreading. This might be because the contact pressure of a spreading droplet is lower in the middle to peripheral regions than in the center region (Ref 5, 24, 25), resulting in the dimples being not filled. The dimples locating at the center region of the splat were filled by the splat.

To understand the differences in morphology of the SOS and the SOD, we compare them in more detail. Figure 8(a) shows another example of the SOD. The droplet forming this splat was 57 μm in diameter and impacted at the speed of 43 m/s and the temperature of 2787 K. For comparison, the SOS that was formed by a droplet almost identical to the one impacting on the dimple was shown in Fig. 8(b). The diameter, velocity, and temperature of this droplet were 58 μm , 43 m/s, and 2779 K, respectively. The average diameter D_{avg} of the central adhered region of the SOD is 189 μm ; hence, the degree of flattening for this region is 3.3. The value of D_{avg} is calculated from the area of splat, S , utilizing $D_{\text{avg}} = \sqrt{4S/\pi}$. Meanwhile, the diameter of the SOS was 183 μm ; hence, the degree of flattening was 3.1. As we see in Fig. 7, here the SOD also flattened more than the SOS.

To study the spreading behavior, the intensity histories of thermal emissions of the SOS and the SOD were compared. Figure 9(a) shows the output voltages of a photomultiplier detecting 700-nm-wavelength thermal

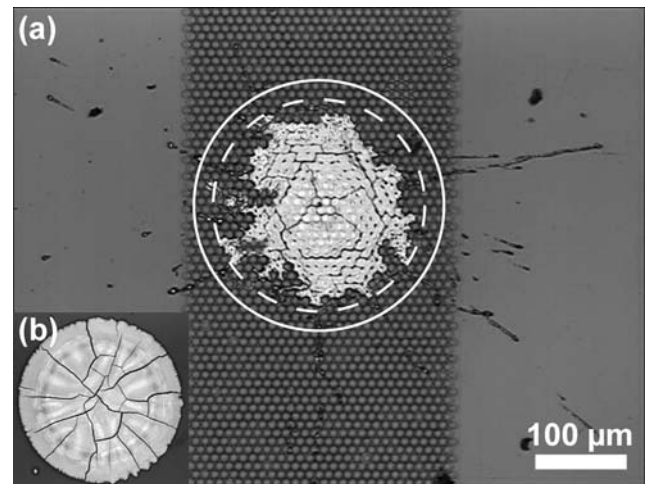


Fig. 8 Laser-scanning microscope views of splats: (a) on dimple-pattern substrate and (b) on smooth substrate. Scale bar in (a) is also valid for (b). The maximum extent of the droplet spread is considered to be between two circles indicated by the solid and dashed lines

emissions of the SOS and the SOD as a function of time. The intensity of detected signals begin to increase approximately 15 μs before droplet impact, indicating that the in-flight droplet has entered the field of view of the condenser lenses used for monitoring the droplet impact. At this time, the droplet is approximately 650 μm above the substrate. The intensity difference in the in-flight region might be due to the difference in reflectivity of substrate surfaces. Assuming that the intensity at $t=0$, I_o , corresponds to the initial droplet size, the intensity history can be normalized by I_o , as shown in Fig. 9(b). Following impact, the intensity increases as the droplet spreads, due to the increase in the area emitting the thermal radiation. After reaching its maximum, I_m , the intensity begins to decay due to the cooling of splat and/or splashing.

Assuming that the intensity becomes maximum when the droplet reaches its maximum spread diameter D_m , the spread time and ξ can be determined, although in some

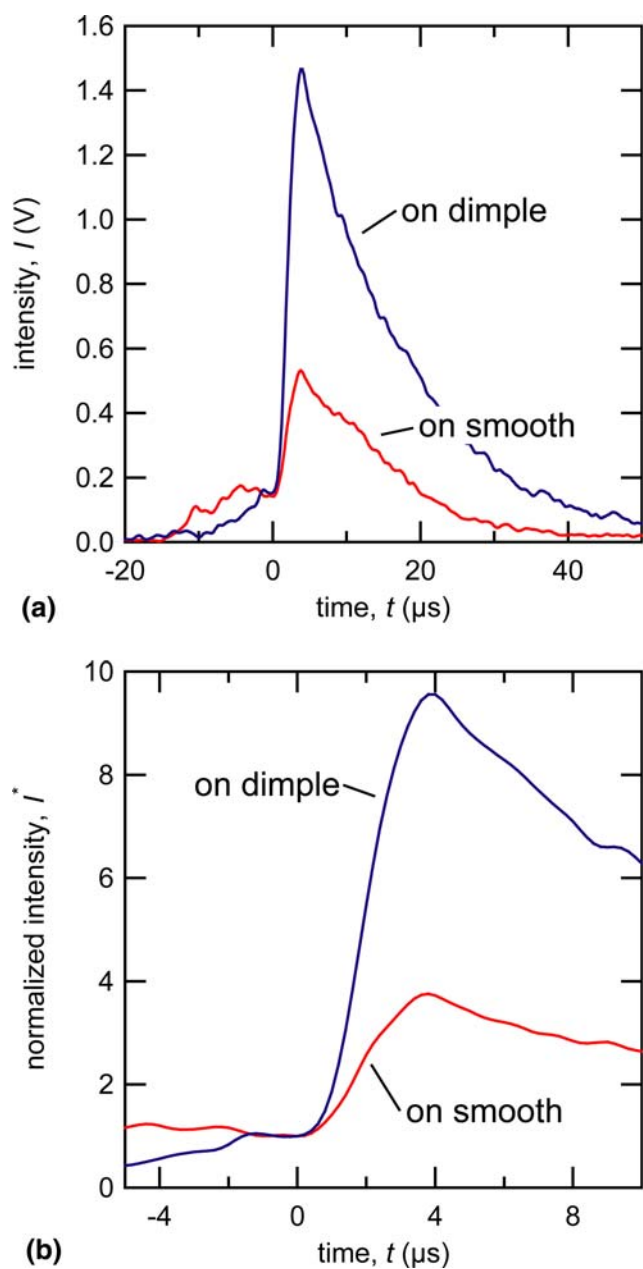


Fig. 9 (a) Comparison of an intensity history I during droplet impact on a dimple pattern with that of a disk-shaped splat on a smooth substrate obtained by a photomultiplier at the wavelength of 700 nm. Time $t = 0$ indicates when the droplet impinged on the substrate. (b) Normalized intensity I^* normalized by the intensity at time $t = 0$ (color online)

cases this may not hold as discussed elsewhere (Ref 26). Based on this assumption, the spreading time of the splat, t_s , on smooth and patterned substrates are 3.8 and 4.0 μs , respectively. Considering the angle of condenser lens through $D_m/d_0 = \sqrt{I_m/I_0} \sin 20^\circ$, the maximum degree of flattening, ξ_m , of the splat on smooth and patterned substrates are calculated as 3.3 and 5.3, respectively.

For the splat on a smooth substrate, the values of ξ measured from thermal emission and by a laser-scanning

microscope agreed very well, as McDonald et al. reported for the case of molybdenum and amorphous steel splats (Ref 27). On the dimple-patterned substrate, however, the ξ measured from the thermal emission was much greater than that from the microscope. In Fig. 8(a), the maximum spread area of the droplet is shown by the solid-line circle; this area was calculated using the thermal radiation signal, assuming that the droplet spreads as a circular thin film. The dashed-line circle in Fig. 8(a) shows the maximum spread area calculated from the laser-scanning microscope measurement, assuming that the error of measured volume was the maximum. In either case, the difference in ξ suggests that the thin liquid film was probably spreading up to this circle area and then ruptured into fingers.

Next, we present the average contact line velocity, V_{avg} , of droplets on different substrates, which was estimated from the spreading time through $V_{\text{avg}} = D_m/t_s$. On the smooth and dimple-patterned substrates, the values of V_{avg} were 51 and 75 m/s, respectively, i.e., on the dimple-patterned substrate the droplet spread approximately 1.5 times faster than on the smooth substrate. It is particularly worth noting that the spread velocity on the patterned substrate was higher than that on the smooth substrate even at the initial stage of the spreading process, as evident from the gradient of the normalized intensities shown in Fig. 9(b).

The initial cooling rate of the SOD was 2.3×10^7 K/s; hence, the apparent thermal contact resistance on the assumption of Newtonian cooling (Ref 20) was 9.3×10^{-6} m² K/W. Meanwhile, the initial cooling rate of the SOS was 8.8×10^7 K/s; hence, the apparent thermal contact resistance was 2.6×10^{-6} m² K/W. Consequently, the thermal contact resistance of the SOD was more than three times larger than that of the SOS. It is natural to think that this difference came from the existence of dimples, because intrinsic thermal contact resistance should be the same at the same impact condition. In addition to the microscope observations, this fact also suggests that the droplet was spreading without filling the dimples. The apparent contact area was much smaller than the splat size because of the dimples, and it can cause higher thermal contact resistance in the case of on the SOD.

Thus, most probably the advancing liquid sheet of the droplet spreading on the dimple-patterned substrate spread without filling the dimples. This is consistent with the simulation result that the droplet did not fill the dimples. The dimples in the central region were probably filled by the subsequent stagnation flow, which was not confirmed by the numerical simulation yet.

4. Discussion

4.1 Comparison Between Numerical Simulation and Experiment

We first compare the results of numerical simulations of the droplet on smooth substrate with experiments. The calculated splat diameter was well consistent with that

observed experimentally; the error was $<10\%$, which is within measurement errors. Next, we consider the results on the dimple-patterned substrates. As discussed earlier, unlike what was observed experimentally, the simulation results for the droplet on the dimple-patterned substrate showed no splashing, although the rim of the splat showed perturbations due to the substrate surface morphology. It was only when the droplet viscosity was lowered that we observed splashing in the simulations. This is probably because the high viscosity suppresses an increase in the velocity difference along the circumference of the advancing liquid sheet. Thus, viscosity of spreading material is the important factor to cause the fingering/splashing.

The other difference between the numerical and experimental results was in the spread velocity of droplets on the dimple-patterned substrates: In the experiments, the spread velocity of droplets on the dimple-patterned substrate was higher than that on the smooth substrate in the initial stages of spreading. However, in the simulations, there was no distinct difference between spread velocities in the initial stages of spreading.

Our explanation for these differences is that it is most likely the air inside dimples that assists a droplet (liquid film) to slip on the dimple surface, and as a result the droplet spread velocity increases on the patterned substrate. Therefore, since the numerical model did not include the effects of surrounding air, it could not capture this effect. A numerical model that can solve two phase flow, i.e., droplet and the surrounding air, will give better representation on this splashing phenomenon on the concave-patterned substrates.

By comprehensive approach between the experiment and numerical simulation, we have approached the splashing phenomenon on concave-patterned substrates. The simulation results clearly indicate the importance of viscosity on disk-shape spreading or fingering/splashing criterion and imply the importance of surrounding air.

4.2 Splashing on Concave Pattern

As presented earlier, droplet splashing occurs on both convex- and concave-patterned substrates. In the case of the convex patterns, a step at a surface triggers droplet splashing (Ref 28). In contrast, in the case of concave patterns, surface grooves cause the slipping of a spreading droplet. When a droplet is spreading with contacting on a smooth region, there will be a large velocity gradient in the direction perpendicular to the substrate. Therefore, the droplet rapidly decelerates due to the viscous dissipation. On the contrary, when a droplet is spreading with slipping over dimples, there will be a less velocity distribution in the perpendicular direction. Thus, the droplet can keep spreading with less deceleration. This spread difference can cause the instability, which leads to fingering/splashing of the droplet. Since the degree of viscous dissipation depends on the viscosity of the spreading droplet, the viscosity can be critical for this instability as the simulation showed.

The dimples may also impede fluid flow by a pinning effect, resulting in lower degree of flattening. Parizi et al.

(Ref 6) showed that a spreading liquid film was impeded by obstacles; a small liquid jet penetrated the space between the obstacles, resulting in fingering. In fact, our simulation also indicated that the minimum speed of the spreading droplet on the dimple pattern was lower than that on the smooth substrate as shown in Fig. 4. Thus, the dimples can either promote spreading by slipping of the spreading droplet or impede fluid flow by pinning phenomena in principle. However, in our experimental regions, the slipping effect seems more significant than the impeding effect. This is supported by the fact that the maximum degree of flattening on the dimple-patterned substrate was larger than that on the smooth substrate. This slipping/impeding effect ratio will change, depending on the balance between the dimple geometry and the droplet impact condition; the impeding effect will be more significant at lower impact speeds.

Xu (Ref 29) classified droplet splashing modes into two types: a corona splash caused by the air surrounding the drop, and a prompt splash caused by the roughness and texture of the surfaces. On a cold substrate, we previously reported that the splashing of an YSZ splat could be a combination of these two effects (Ref 26). Previous studies suggest that the surface adsorbates enhance splashing on a cold substrate. However, in the scale of plasma-sprayed particles under extreme conditions, these effects come together and are indistinguishable. As an example for such distinguishable splashing, Fig. 10 shows a splat on an oxide photonic crystal preheated to 700 K. The substrate has high-aspect-ratio-columnar structures that have a few hundred nanometer columns, which were an order of magnitude smaller than the patterns of quartz glass substrates used in this study. This high-aspect ratio pattern can be regarded as an extreme concave pattern. As can be seen, the droplet completely splashed very similar to the splat morphology on the cold substrate. Note that this splash is not caused by surface adsorbates, because the adsorbates almost vanish on a substrate preheated to

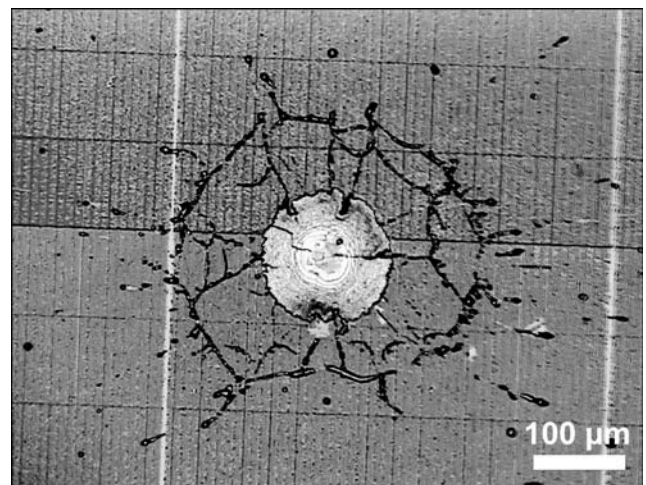
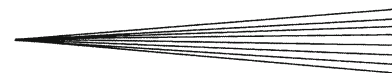


Fig. 10 Laser-scanning microscope view of a splat on a high-aspect-micropatterned substrate



700 K. Thus, the splash of a droplet on a concave pattern should be considered separately from the prompt splash, which can be caused by the surface roughness; the air inside the concaves enhances the slip of the spreading droplet and may play an important role in the splash.

Another unanswered question of this study is whether the advancing liquid sheet of a droplet can be ejected before the main flow and shortly after impact in plasma spray, as reported by Thoroddsen et al. for water droplets (Ref 30-32). Thoroddsen et al. reported that this sheet is ejected even at impact velocities less than ultrasonic velocities like plasma spray process. At least, when a droplet impacts at much higher temperatures and the viscosity of the droplet becomes a magnitude of order smaller than this study, the emergence of the advancing liquid sheet can occur, which remains as a future assignment.

Finally, the effect of solidification on the spread is considered. Our results suggest that the thermal contact resistance becomes larger on the dimple-pattern substrates because the dimples below the splat were not fully filled, and it gives poor contact between the splat and the substrate. As Dhiman et al. (Ref 19) suggested, in the case of YSZ, contribution of the solidification to the splashing would be rather small, because of the lower solidification rate. Thus, it is expected that the effect of solidification is minor in the combination of YSZ droplets and concave patterns. Whatever the case may be, the design of concave patterns can affect the splat formation in terms of both fluid dynamics and heat transfer. This may help the control of the spreading behavior of the droplet in plasma spraying, which is already achieved in polymer liquid spread (Ref 33) and shown by simulation (Ref 7).

5. Conclusions

The effects of concave patterns of the substrate on the spreading behaviors of YSZ particles were investigated both numerically and experimentally under hybrid-plasma spraying conditions. The micrometer-scale dimple-patterns caused fingering/splashing of impacting droplets in plasma spraying. The main mechanism that causes splashing is likely due to the slip of the spreading droplet at the concave regions. As numerical simulation suggested, the fingering/splashing occurred only when the viscosity of the spreading droplet was decreased. Below a certain viscosity, the instability of spreading droplet increased and caused the fingering/splashing. Thus, concave aspects of a substrate surface play an important role in splashing of spreading droplet over that surface as well as convex patterns in plasma spraying.

Acknowledgments

The simulations and experiments in this study were conducted at the University of Toronto and the University of Tokyo, respectively. We appreciate Mr. Atsushi Yamada

(Graduate Student of the University of Tokyo, currently Honda R&D Co.) for providing the micropatterned substrates for the experiments. We also appreciate Dr. Seiji Kuroda (National Institute for Materials Science) for useful discussions.

References

1. T. Yoshida, Toward a New Era of Plasma Spray Processing, *Pure Appl. Chem.*, 2006, **78**(6), p 1093-1107
2. S. Chandra and P. Fauchais, Formation of Solid Splats During Thermal Spray Deposition, *J. Therm. Spray Technol.*, 2009, **18**(2), p 148-180
3. K. Shinoda, A. Yamada, M. Kambara, Y. Kojima, and T. Yoshida, Deformation of Alumina Droplets on Micro-Patterned Substrates under Plasma Spraying Conditions, *J. Therm. Spray Technol.*, 2007, **16**(2), p 300-305
4. A. McDonald, L. Rosenzweig, S. Chandra, and C. Moreau, Impact of Plasma-Sprayed Particles on Textured Silicon Wafers, *Proceedings of the 20th Annual Conference on Liquid Atomization and Spray Systems*, May 15-18, 2007 (Chicago, IL), ILASS Americas, 2007, Art. No. 58 (8 p)
5. A. McDonald, S. Chandra, and C. Moreau, Photographing Impact of Plasma-Sprayed Particles on Rough Substrates, *J. Mater. Sci.*, 2008, **43**(13), p 4631-4643
6. H.B. Parizi, L. Rosenzweig, J. Mostaghimi, S. Chandra, T. Coyle, H. Salimi, L. Pershin, A. McDonald, and C. Moreau, Numerical Simulation of Droplet Impact on Patterned Surfaces, *J. Therm. Spray Technol.*, 2007, **16**(5-6), p 713-721
7. M. Raessi, J. Mostaghimi, and M. Bussmann, Effect of Surface Roughness on Splat Shapes in the Plasma Spray Coating Process, *Thin Solid Films*, 2006, **506**, p 133-135
8. N. Ferguen, P. Fauchais, A. Vardelle, and D. Gobin, Numerical Investigation of Impact and Solidification of YSZ Droplets Plasma-Sprayed onto a Substrate: Effect of Thermal Properties and Roughness, *Ceram. Eng. Sci. Proc.*, 2009, **29**(4), p 159-170
9. A.M. Ahmed and R.H. Rangel, Metal Droplet Deposition on Non-Flat Surfaces: Effect of Substrate Morphology, *Int. J. Heat Mass Trans.*, 2002, **45**(5), p 1077-1091
10. M. Bussmann, J. Mostaghimi, and S. Chandra, On a Three-Dimensional Volume Tracking Model of Droplet Impact, *Phys. Fluids*, 1999, **11**(6), p 1406-1417
11. M. Pasandideh-Fard, S. Chandra, and J. Mostaghimi, A Three-Dimensional Model of Droplet Impact and Solidification, *Int. J. Heat Mass Trans.*, 2002, **45**(11), p 2229-2242
12. Y. Cao, A. Faghri, and W.S. Chang, A Numerical Analysis of Stefan Problems for Generalized Multi-Dimensional Phase-Change Structures Using Enthalpy Transforming Model, *Int. J. Heat Mass Trans.*, 1989, **32**(7), p 1289-1298
13. Y.K. Chae, J. Mostaghimi, and T. Yoshida, Deformation and Solidification Process of a Super-Cooled Droplet Impacting on the Substrate under Plasma Spraying Conditions, *Sci. Technol. Adv. Mater.*, 2000, **1**(3), p 147-156
14. M.W. Chase, Jr., Ed., NIST-JANAF Thermochemical Tables, 4th ed., *J. Phys. Chem. Refer. Data*, **9**, American Chemical Society, and American Institute of Physics for the National Institute of Standards and Technology (New York), 1951 p
15. J.M. Lihmann and J.S. Haggerty, Surface Tensions of Alumina-Containing Liquids, *J. Am. Ceram. Soc.*, 1985, **68**(2), p 81-85
16. M. Vardelle, A. Vardelle, A.C. Leger, P. Fauchais, and D. Gobin, Influence of Particle Parameters at Impact on Splat Formation and Solidification in Plasma Spraying Processes, *J. Therm. Spray Technol.*, 1995, **4**(1), p 50-58
17. K. Shinoda, Y. Kojima, and T. Yoshida, In Situ Measurement System for Deformation and Solidification Phenomena of Yttria-Stabilized Zirconia Droplets Impinging on Quartz Glass Substrate under Plasma Spraying Conditions, *J. Therm. Spray Technol.*, 2005, **14**(4), p 511-517
18. M. Pasandidehfard and J. Mostaghimi, On the Spreading and Solidification of Molten Particles in a Plasma Spray Process:

- Effect of Thermal Contact Resistance, *Plasma Chem. Plasma Process.*, 1996, **16**(1), p S83-S98
19. R. Dhiman, A.G. McDonald, and S. Chandra, Predicting Splat Morphology in a Thermal Spray Process, *Surf. Coat. Technol.*, 2007, **201**(18), p 7789-7801
 20. K. Shinoda, T. Koseki, and T. Yoshida, Influence of Impact Parameters of Zirconia Droplets on Splat Formation and Morphology in Plasma Spraying, *J. Appl. Phys.*, 2006, **100** (7), Art. No. 074903 (6 p)
 21. T. Yoshida, T. Okada, H. Hamatani, and H. Kumaoka, Integrated Fabrication Process for Solid Oxide Fuel Cells Using Novel Plasma Spraying, *Plasma Sour. Sci. Technol.*, 1992, **1**(3), p 195-201
 22. T. Yoshida, T. Tani, H. Nishimura, and K. Akashi, Characterization of a Hybrid Plasma and Its Application to Chemical Synthesis, *J. Appl. Phys.*, 1983, **54**(2), p 640-646
 23. K. Shinoda, P. Han, and T. Yoshida, The Microstructure of YSZ Splats Deposited by Hybrid Plasma Spraying, *Proceedings of the 15th International Symposium on Plasma Chemistry*, A. Bouchoule, J.M. Pouvesle, A.L. Thomann, J.M. Bauchire, and E. Robert, Ed., Vol. VI, July 9-13, 2001 (Orléans, France), GREMI, CNRS/University of Orléans, 2001, p 2661-2666
 24. D. Sivakumar, K. Katagiri, T. Sato, and H. Nishiyama, Spreading Behavior of an Impacting Drop on a Structured Rough Substrate, *Phys. Fluids*, 2005, **17**(10), Art. No. 100608 (10 p)
 25. C.J. Li and J.L. Li, Transient Contact Pressure During Flattening of Thermal Spray Droplet and Its Effect on Splat Formation, *J. Therm. Spray Technol.*, 2004, **13**(2), p 229-238
 26. K. Shinoda, H. Murakami, S. Kuroda, S. Oki, K. Takehara, and T.G. Etoh, High-Speed Thermal Imaging of Yttria-Stabilized Zirconia Droplet Impinging on Substrate in Plasma Spraying, *Appl. Phys. Lett.*, 2007, **90** (19), Art. No. 194103 (3 p)
 27. A. McDonald, M. Lamontagne, C. Moreau, and S. Chandra, Impact of Plasma-Sprayed Metal Particles on Hot and Cold Glass Surfaces, *Thin Solid Films*, 2006, **514**(1-2), p 212-222
 28. C. Josserand, L. Lemoine, R. Troeger, and S. Zaleski, Droplet Impact on a Dry Surface: Triggering the Splash with a Small Obstacle, *J. Fluid Mech.*, 2005, **524**, p 47-56
 29. L. Xu, Liquid Drop Splashing on Smooth, Rough, and Textured Surfaces, *Phys. Rev. E*, 2007, **75**, Art. No. 056316 (8 p)
 30. S.T. Thoroddsen, The Ejecta Sheet Generated by the Impact of a Drop, *J. Fluid Mech.*, 2002, **451**, p 373-381
 31. S.T. Thoroddsen, T.G. Etoh, K. Takehara, and Y. Takano, Impact Jetting by a Solid Sphere, *J. Fluid Mech.*, 2004, **499**, p 139-148
 32. S.T. Thoroddsen and J. Sakakibara, Evolution of the Fingering Pattern of an Impacting Drop, *Phys. Fluids*, 1998, **10**, p 1359-1374
 33. L. Courbin, E. Denieul, E. Dressaire, M. Roper, A. Ajdari, and H.A. Stone, Imbibition by Polygonal Spreading on Microdecorated Surfaces, *Nat. Mater.*, 2007, **6**(9), p 661-664